Available online at www.sciencedirect.com
ScienceDirect
Journal of the European Ceramic Society 30 (2010) 561–567
www.elsevier.com/locate/jeurceramsoc

Percolative $BaTiO_3$–Ni composite nanopowders from alkoxide-mediated synthesis

Songhak Yoon [a,*], Jürgen Dornseiffer [b], Theo Schneller [c], Detlev Hennings [a], Shoichi Iwaya [d,e], Christian Pithan [a], Rainer Waser [a,c]

[a] *Institut für Festkörperforschung, Forschungszentrum Jülich GmbH, D-52425 Jülich, Germany*
[b] *Institut für Chemie und Dynamik der Geosphäre, Forschungszentrum Jülich GmbH, D-52425 Jülich, Germany*
[c] *Institut für Werkstoffe der Elektrotechnik, RWTH Aachen, D-52056 Aachen, Germany*
[d] *IOM Technology Corporation, 957-0231 Shibata-shi, Japan*
[e] *Technical R&D Division, NAMICS CORPORATION, 108-0074 Tokyo, Japan*

Available online 9 July 2009

Abstract

$BaTiO_3$–Ni nanopowders have been synthesized via an alkoxide-mediated synthesis route through the hydrolysis and condensation of barium hydroxide octahydrate and titanium (IV) isopropoxide in the presence of submicron sized, spherical Ni particles originating from a commercial Ni paste, that was introduced during the preparation procedure. X-ray diffraction (XRD) patterns indicate that nanocomposite powders of the phases $BaTiO_3$ and Ni could be successfully prepared and tailor-made composition control was confirmed. Scanning electron microscopy (SEM) and transmission electron microscopy (TEM) show that the synthesized $BaTiO_3$ nanoparticles were aggregates of nanosized primary particles as small as 40 nm in diameter. The average Ni particle size was estimated to be about 200 nm. Dilatometric measurements on green compacts of these powders revealed that the shrinkage of $BaTiO_3$–Ni composites is retarded compared to both, pure $BaTiO_3$ and Ni. Thermogravimetric analysis (TGA) shows weight losses due to the decomposition of organic binder from Ni paste, the release of water from the surface and of hydroxyl ions from inside the lattice of the $BaTiO_3$ nanoparticles. With the addition of nickel, the dielectric constant increased slightly due to the percolation effect.

Keywords: Composites; $BaTiO_3$; Dielectric properties; Alkoxide-mediated synthesis; Sintering

1. Introduction

Nanocomposites are composite materials in which one of the phases has dimensions in the nanometer range.[1] Nanocomposite materials have been extensively explored for many technological applications due to specific combinations of mechanical, optical, catalytic, electrical or magnetic properties with fundamentally different properties that cannot be achieved for single phase, pure materials.[2–4] Ceramic–metal nanocomposites are promising candidate materials for fabricating multifunctional nanodevices due to sometimes outstanding electrical properties with very particular features.[5,6] In order to realize an optimized microstructure for ceramic–metal nanocomposites, much effort has been undertaken concerning the control of the size and distribution of the metal nanoparticles.

From the theoretical point of view the dielectric behavior of ferroelectric–metal composites has attracted much attention for many years due to the extraordinary dielectric constant enhancement, that can be anticipated when metal inclusions are distributed in an insulating ceramic matrix.[7–10] According to theory, only in the vicinity just below the percolation threshold the enhancement of the dielectric constant is abnormally large. Up to the present it was very difficult to experimentally observe the phenomena occurring directly at the percolation threshold and only a few groups have reported the effect of a strongly enhanced dielectric constant for ceramic–metal composites in the neighborhood of the percolation threshold.[11–16] Only microcomposites, however, have been reported in the literature up to now. A more efficient approach to the percolative threshold, for which the highest performance is anticipated, can be achieved for much more intimate and homogeneous mixtures of the dielectric and conductive phases. In order to understand the microscopic origin of the dielectric properties and to further enhance the dielectric constant, the feasibility of

* Corresponding author. Tel.: +49 2461 61 5016; fax: +49 2461 61 2550.
E-mail address: s.yoon@fz-juelich.de (S. Yoon).

0955-2219/$ – see front matter © 2009 Elsevier Ltd. All rights reserved.
doi:10.1016/j.jeurceramsoc.2009.06.024

the preparation of homogeneous mixtures of ceramic and metal nanoparticles should be investigated. This is the objective of the present study, which focuses on the system $BaTiO_3$–Ni.

A number of publications have appeared in the literature on the alkoxide–hydroxide process, since Flaschen first proposed the synthesis of crystalline barium titanate and there are several modifications of the experimental procedures.[17–21] The alkoxide–hydroxide route has the merit that crystalline $BaTiO_3$ nanoparticles can be easily synthesized at a low temperature below 100 °C without any further calcinations. By means of the proper control of experimental parameters, pure $BaTiO_3$ nanopowders have been successfully prepared applying the alkoxide–hydroxide synthesis.[22,23] It is believed that a rationally modified synthetic route can also be adapted for the preparation of $BaTiO_3$–Ni composite nanopowders. Up to date, no publication has reported about an alkoxide-mediated route for the synthesis of $BaTiO_3$–metal composite nanopowders.

In this study, a new class of $BaTiO_3$–Ni composite nanopowders has therefore been synthesized via alkoxide-mediated synthesis. This modified synthetic route has been developed in order to prepare homogeneously dispersed Ni metal nanoparticles in a matrix of $BaTiO_3$ and to clarify the correlation between the composite microstructure and electrical properties. The microstructure evolution, sintering behavior and electrical properties are investigated.

2. Experimental procedures

$BaTiO_3$–Ni composite nanopowders were synthesized under N_2 atmosphere through an alkoxide–hydroxide sol-precipitation method. During the hydrolysis and condensation of barium hydroxide octahydrate ($Ba(OH)_2{\cdot}8H_2O$; 98+%, Alfa Aesar, Karlsruhe, Germany) and titanium (IV) isopropoxide ($Ti[OCH(CH_3)_2]_4$, 97+%, Alfa Aesar, Karlsruhe, Germany), an alcoholic dilution of a commercial Ni paste (X6428U-1, NAMICS, Japan) was introduced. Because the alkoxides and hydroxides are extremely sensitive to CO_2 and moisture, the entire preparation of the reactants for the synthesis was performed in a glove box filled under purified argon gas (H_2O content: <1 ppm, O_2 content: <2 ppm, M. Braun Inertgas-Systeme GmbH, Garching, Germany).

Different amounts of Ni paste were dissolved in respectively 6 mol of dried isopropanol (C_3H_7OH, 99.8%, Merck KGaA, Darmstadt, Germany) at room temperature. An ultrasonic homogenizer (SONOPULS, BANDELIN, Berlin, Germany) was used for 10 min in order to disperse the metal particles. Titanium (IV) isopropoxide (0.03 mol) was added in this solution followed by dispersion for 10 min by ultrasonic homogenization. In the meantime, barium hydroxide octahydrate (0.03 mol) was added to deionized degassed water (18 mol) at room temperature while stirring vigorously. Then the water mixture solution of barium hydroxide octahydrate was heated to 80 °C at the rate of 2 °C/min. As soon as the solution temperature reached at 80 °C, the as-prepared isopropanolic solution of Ni paste and titanium (IV) isopropoxide was slowly added. Seven different $BaTiO_3$–Ni composite nanopowders with different volume fractions of Ni were prepared: 0, 5, 10, 15, 20, 23, 25, and 27%.

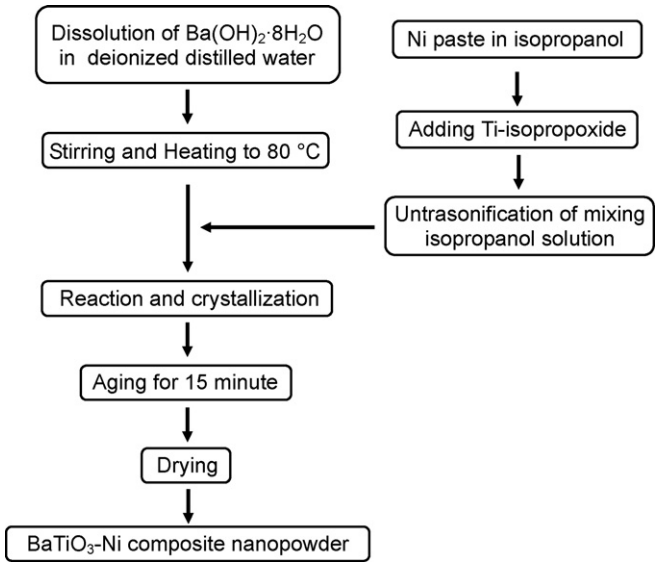

Fig. 1. Flow chart for the synthesis of $BaTiO_3$–Ni composite nanopowders using an alkoxide-mediated method.

After 15 min of refluxing at 80 °C, the solutions were decanted and dried at 80 °C for 12 h. Fig. 1 represents the flow chart of the applied alkoxide-mediated method for the synthesis of $BaTiO_3$–Ni composite nanopowders.

With the synthesized composite powders, phase identification was performed by powder X-ray diffraction (XRD, Philips X'PERT, Koninklijke Philips Electronics N.V., Eindhoven, the Netherlands) using Cu-Kα radiation with a wavelength of $\lambda = 1.5418$ Å. The respective diffraction patterns were recorded in scans from 20 to 100 (2θ) using an angular step interval of 0.01°. The X-ray diffraction patterns obtained were analyzed by the Rietveld refinement program, Fullprof,[24] in order to determine the lattice parameter and crystallite size of the as synthesized $BaTiO_3$–Ni powder. Thompson-Cox-Hastings pseudo-Voigt functions were chosen as profile function among all the profiles in the Fullprof program.

The particle size and distribution of the synthesized composite nanopowders were also characterized by field emission scanning electron microscopy (FE-SEM, LEO1530, Carl Zeiss AG, Jena, Germany) operating at 20 kV and transmission electron microscopy (TEM, CM-200, Koninklijke Philips Electronics N.V.) operating at 200 kV. Samples for SEM and TEM were prepared by dropping the synthetic mixture solution obtained after 15 min at 80 °C on the carbon-coated copper grids.

The sintering behavior of the raw powders was investigated using dilatometry (DIL 402 C, Netzsch Gerätebau GmbH, Germany) under Ar atmosphere in the temperature range from 25 to 1050 °C. For this purpose pellets were compacted by uniaxial pressing applying 5 kN to a cylindrical steel die (10 mm diameter) followed by cold isostatic pressing at 425 kN (Weber Pressen KIP 40ES, Paul-Otto Weber GmbH, Remshalden, Germany). The heating and cooling rate of the dilatometer was 20 °C/min, respectively. Thermogravimetric analysis (TGA, STA 429, Netzsch Gerätebau GmbH, Selb,

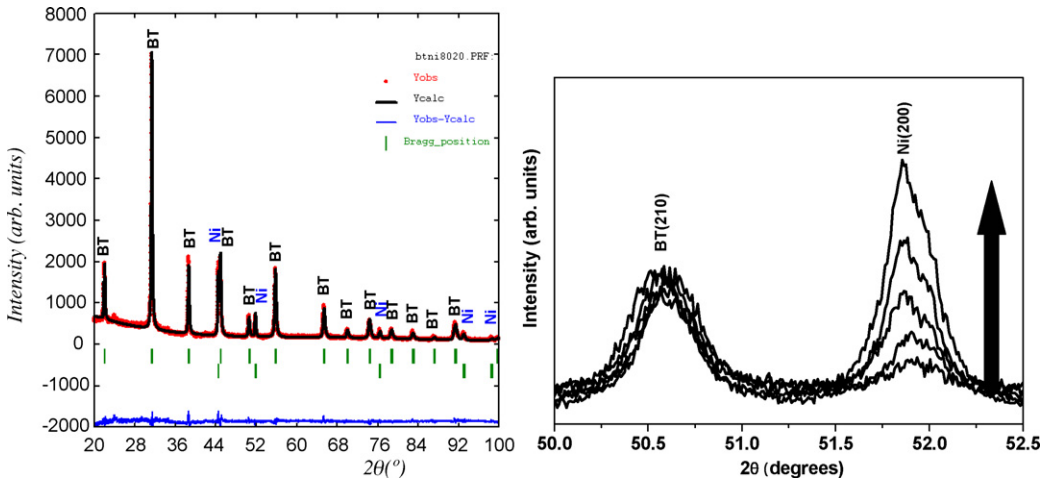

Fig. 2. XRD patterns of the synthesized $BaTiO_3$–Ni composite nanopowders. (a) Full pattern of $BaTiO_3$–Ni (20 vol.% of nickel), (b) with nickel volume fraction $f = 5$, 10, 20, 25 and 27 vol.%.

Germany) experiments were carried out under Ar atmosphere in a temperature range from 25 to 1050 °C with a heating and cooling rate of 20 °C/min, respectively.

For the electrical measurements Au was deposited onto the sintered pellets as electrodes by thermal evaporation method and silver was painted on for wire bonding. The wires of the samples were connected via the "Test Fixture" HP16047A to the impedance analyzer (Hewlett Packard, type 4284A). Dielectric properties of the samples were measured at room temperature at a frequency of 100 kHz with a 10 V AC small signal.

3. Results and discussion

Fig. 2(a) shows the X-ray diffraction patterns of the $BaTiO_3$–Ni composite nanopowders with 20 vol.% of nickel. All peaks were attributed to either the phase $BaTiO_3$ or Ni without any other reflections due to impurity phases being observed, suggesting that no reaction took place between $BaTiO_3$ and Ni during the synthesis. The relative diffraction intensity of the Ni reflections increased with the increase of Ni content as shown in Fig. 2(b) for the case of (2 0 0). This evolution of the XRD-peaks confirms the tailor-controlled composition during the synthesis

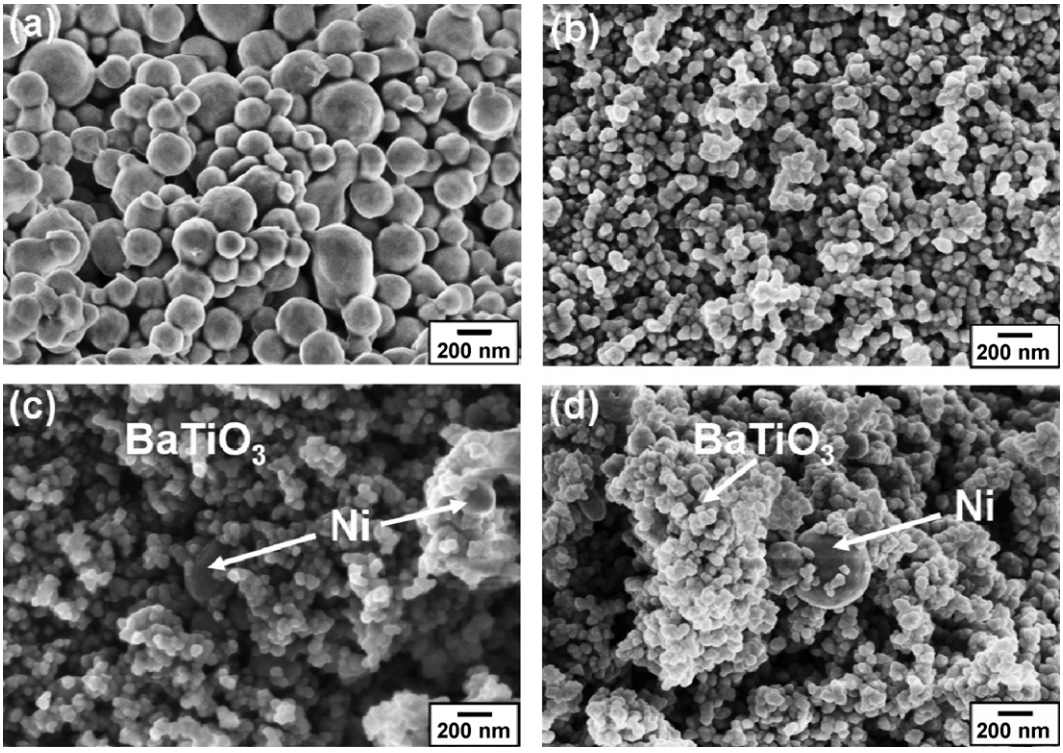

Fig. 3. SEM micrographs of synthesized $BaTiO_3$–Ni composite nanopowders: (a) Ni paste, (b) $BaTiO_3$, (c) 10, and (d) 20 vol.% of nickel fraction.

Table 1
Refined crystal size, lattice parameters and reliability factors of all XRD patterns of the $BaTiO_3$–Ni composite nanopowders.

Ni content (%)	Crystal size (nm)		Lattice parameter (Å)		Reliability factor	
	$BaTiO_3$	Ni	$BaTiO_3$	Ni	R_{WP}	χ^2
5	34.63	199.88	4.0347	3.5234	8.77	2.41
10	37.13	175.26	4.0307	3.5233	9.73	2.78
15	35.27	206.29	4.0343	3.5226	9.41	2.23
20	33.23	193.80	4.0313	3.5248	8.46	2.27
23	35.72	192.58	4.0333	3.5220	9.09	2.11
25	38.31	171.56	4.0342	3.5249	10.7	2.83
27	33.40	203.47	4.0373	3.5250	8.65	2.02

R_{WP}: final weighted reliability factor, χ^2: reduced chi-square.

of the prepared $BaTiO_3$–Ni composite nanopowders. The structural refinements were done using Rietveld analysis (least-square method). The refined crystal size, lattice parameters and reliability factors of all XRD patterns are summarized in Table 1. Almost no variation in lattice parameters and crystal size was found for the different material compositions.

The phase morphology and size of as-synthesized $BaTiO_3$–Ni composite powders are shown in Fig. 3. The average Ni particle size was estimated to be about 200 nm (Fig. 3(a)) and that of $BaTiO_3$ was about 40 nm (Fig. 3(b)), which is consistent with the Rietveld analysis of XRD patterns. With the increase of Ni content of the composite powders, we observed that a large number of Ni clusters are homogeneously dispersed in the $BaTiO_3$ matrix forming however significant aggregates of about 1 μm in size, illustrating the difficulty of breaking Ni-aggregates into particles smaller than 1 μm with ultrasonic homogenizing alone during the synthesis. Ni particles covered by the aggregated $BaTiO_3$ nanoparticles can be seen in some area but cannot explicitly identified in SEM as shown in Fig. 3(c) and (d).

Bright-field TEM images of some of the as-synthesized $BaTiO_3$–Ni composite powders are shown in Fig. 4. Individual $BaTiO_3$ nanocrystals can be clearly observed by TEM (Fig. 4(a)), and many microaggregates of Ni nanoparticles with an approximate diameter of about 1 μm appear. These microparticles are composed of nanoparticles about 200 nm in diameter as shown in Fig. 4(b). TEM-observation under high magnifications reveals that thin layers were formed on the surface of Ni particles, representing a clear evidence for a successful coating of the finer $BaTiO_3$ onto Ni (Fig. 4(c)).

Fig. 5 shows the TGA curves of the as-synthesized $BaTiO_3$–Ni composite nanopowders. All weight losses were accomplished below 400 °C for the pure Ni paste due to the decomposition of organic binders. In the $BaTiO_3$–Ni composite powders, the TGA results show several successive steps of mass losses. The first one occurs between room temperature up to approximately 400 °C and is attributed to the burnout of organics and the release of physisorbed water on the surface of the $BaTiO_3$ nanopowders.[25,26] The second weight loss is observed for a wide range of temperatures up to 1000 °C and mainly results from the release of chemisorbed water and/or incorporated hydroxyl ions in the lattice of $BaTiO_3$. It is apparent that with the increase of Ni addition, as-prepared $BaTiO_3$–Ni nanopowders show increased weight losses due to the higher concentrations of organics, water, and hydroxyl ions.

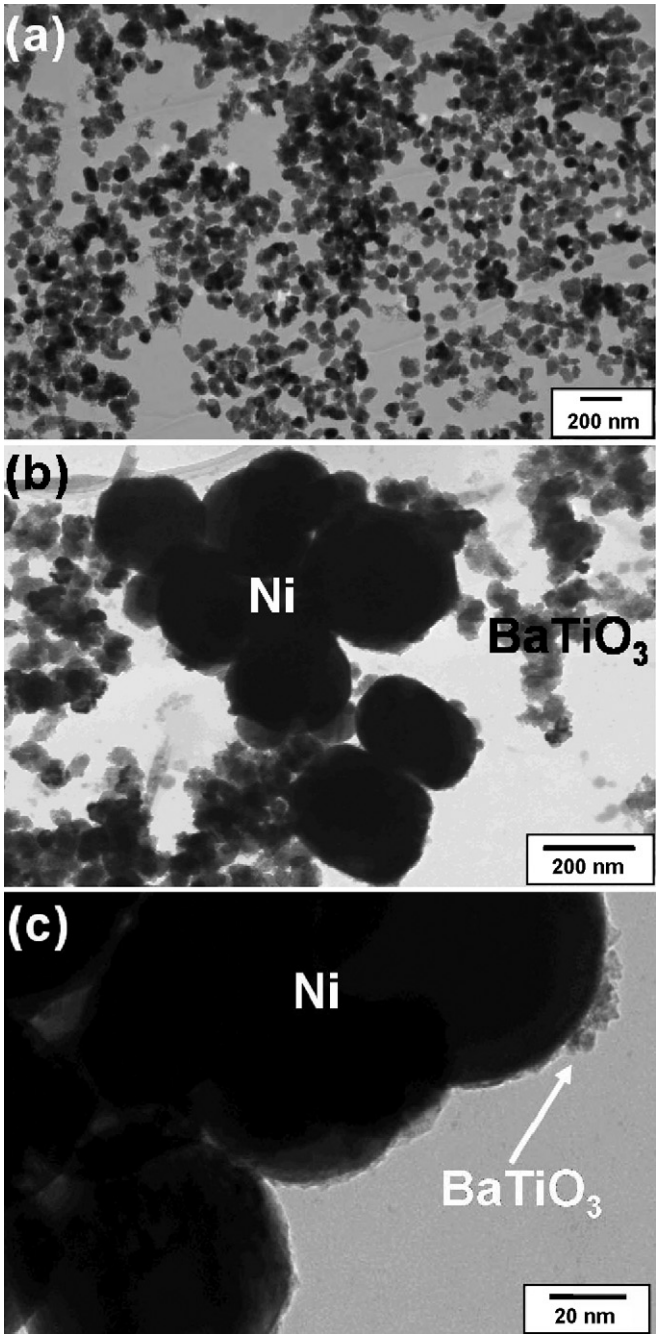

Fig. 4. TEM micrographs of synthesized $BaTiO_3$–Ni composite nanopowders: (a) pure $BaTiO_3$, (b) 10 vol.% of Ni, and (c) 25 vol.% of Ni.

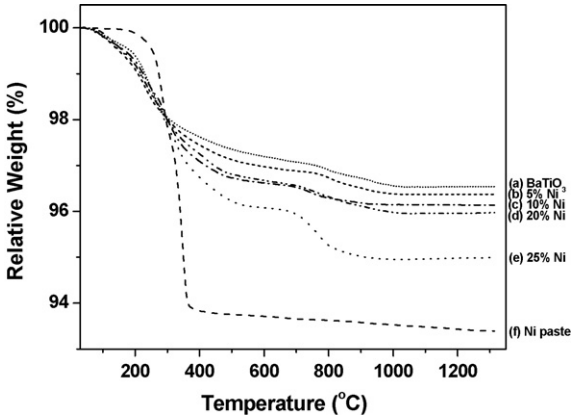

Fig. 5. Thermogravimetric analysis (TGA) of $BaTiO_3$–Ni composite nanopowders with nickel addition: (a) 0, (b) 5, (c) 10, (d) 20, (e) 25 vol.%, and (f) Ni paste (Ar atmosphere with 10 ppm O_2).

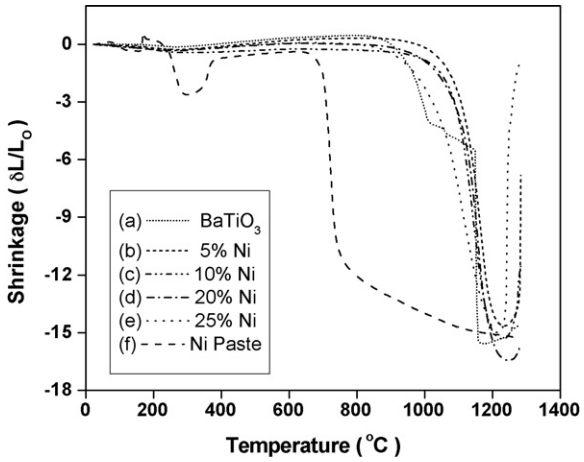

Fig. 6. Dilatometric study of $BaTiO_3$–Ni composite nanopowders with nickel addition: (a) 0, (b) 5, (c) 10, (d) 20, (e) 25 vol.%, and (f) Ni paste (Ar atmosphere with 10 ppm O_2).

Dilatometric measurements were carried out in order to study the sinterability of the synthesized composite nanopowders. The linear shrinkage curves of the samples are presented in Fig. 6. The $BaTiO_3$–Ni composites show a retarded shrinkage behavior compared to both, pure $BaTiO_3$ and Ni. However, the higher the Ni content, the earlier the shrinkage started within the composite. The shrinkage starts at about 900 °C and becomes significant for temperatures above 1000 °C. Above 1200 °C, however, all composites start to expand, probably due to the abnormal grain growth of $BaTiO_3$ and thermal oxidation of the nickel phase. Even though all dilatometric measurements were carried in Ar atmosphere, the obtained nickel nanoparticles in the composite powders were possibly easily oxidized due to the remanant O_2 (10 ppm) in flowing gas.

Fig. 7 shows optical micrographs of sintered $BaTiO_3$–Ni samples with different nickel volume fractions after dilatometry. Strong grain growth of $BaTiO_3$ and Ni is observed and the average grain size of $BaTiO_3$ is about 10 μm. With the addition of Ni, it is apparent that nickel particles agglomerate to form particles of a few micron in size (bright) upon sintering and grain growth.

Fig. 8 shows the dielectric constant of the $BaTiO_3$–Ni composites (dilatometer samples) as a function of the volume

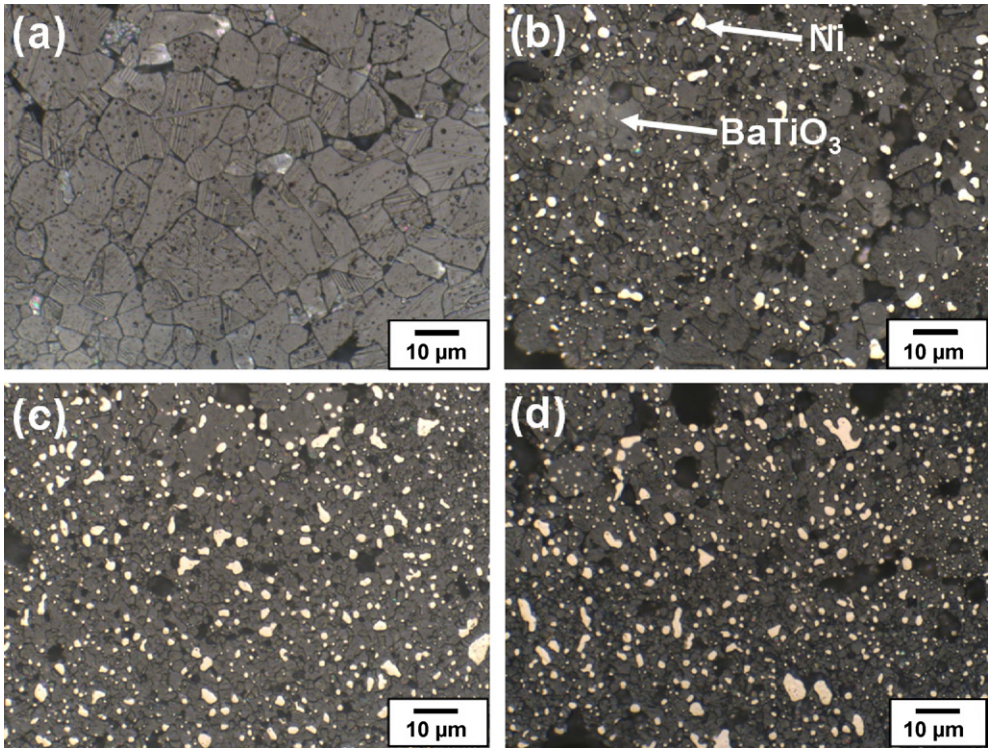

Fig. 7. Optical micrographs of $BaTiO_3$–Ni composites sintered in the dilatometer with different nickel additions: (a) 0, (b) 10, (c) 20, and (d) 25 vol.%.

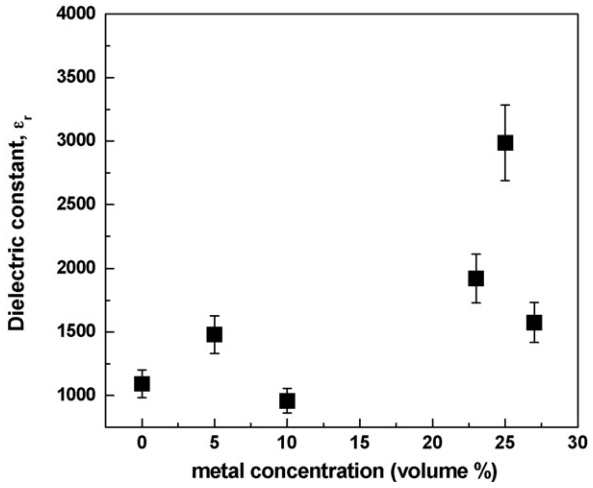

Fig. 8. Plot of the dielectric constant of $BaTiO_3$–Ni composites as a function of the volume fraction of nickel. The data for 20 vol.% of Ni is missing due to a short cut occurring during the measurement.

fraction of nickel. In contrast to the previous reports about the enhancement of dielectric constant in the vicinity of the percolation threshold,[11–16] only a moderate increase was observed upon nickel addition in $BaTiO_3$–Ni composites (error bars in Fig. 8 are within 10% of standard deviation). This can be explained by the poor density of the composites. All composite pellets only show values between 73 and 85% of the theoretical full density. Moreover, nickel particles are slightly oxidized during the dilatometric measurements. It is noted that the effective dielectric field developed around the conducting particles causes an increase in the dielectric constant of ceramic–metal composites.[16] Thus, it is apparent that effective dielectric field was not well formulated in $BaTiO_3$–Ni composite due to the formation of nickel oxide on the surface of nickel particles. It is expected, however, that advanced sintering techniques such as spark plasma sintering will enable the preparation of fully densified percolative $BaTiO_3$–Ni nanocomposite without oxidation of nickel and enhanced dielectric performance. Further studies are underway and will be reported in a separate publication.

4. Summary

$BaTiO_3$–Ni composite nanoparticles were successfully prepared with alkoxide-mediated synthesis. The synthesized $BaTiO_3$ nanoparticles were aggregates of nanosized primary particles as small as 40 nm and the size of Ni nanoparticles was about 200 nm. $BaTiO_3$ nanoparticles were deposited on Ni particles and a rather homogeneous distribution of slightly aggregated Ni particles could be confirmed. Dilatometric analysis of $BaTiO_3$–Ni composite nanopowders revealed that the shrinkage was delayed compared to pure $BaTiO_3$ and Ni. Though enhanced dielectric constant in $BaTiO_3$–Ni composite was not fully achieved due to the poor density and oxidation of nickel, alkoxide-mediated synthetic route show the possibility to be adapted for the preparation of various novel $BaTiO_3$–metal nanocomposite powders for new concepts of electroceramic materials and their potential applications.

Acknowledgements

This work was supported by the Korea Research Foundation Grant funded by the Korean Government (KRF-2007-D00124). The authors are grateful to Mr. Volker Gutzeit for the help related to optical microscopy, Dr. Wessel Egbert for FE-SEM and Dipl.-Ing. Jochen Friedrich for the dilatometric analysis and TGA. NAMICS Corporation, Niigata (Japan) is gratefully acknowledged for financial support within a common collaboration project.

References

1. Roy, R., Roy, R. A. and Roy, D. M., Alternative perspectives on quasi-crystallinity: non-uniformity and nanocomposites. *Mater. Lett.*, 1986, **4**, 323–328.
2. Komarneni, S., Nanocomposites. *J. Mater. Chem.*, 1992, **2**, 1219–1230.
3. Kondo, H., Sekino, T., Tanaka, N., Nakayama, T., Kusunose, T. and Niihara, K., Mechanical and magnetic properties of novel yttria-stabilized tetragonal zirconia/Ni nanocomposite prepared by the modified internal reduction method. *J. Am. Ceram. Soc.*, 2005, **88**, 1468–1473.
4. Moya, J. S., López-Esteban, S. and Pecharromán, C., The challenge of ceramic/metal microcomposites and nanocomposites. *Prog. Mater. Sci.*, 2007, **52**, 1017–1090.
5. Cho, W. W., Kagomiya, I., Kakimoto, K.-I. and Ohsato, H., Paraelectric ceramics/metal dual composites $SrTiO_3$/Pt system with giant relative permittivity. *Appl. Phys. Lett.*, 2006, **89**, 152905.
6. Panteny, S., Bowen, C. R. and Stevens, R., Characterisation of barium titanate–silver composites. Part II. Electrical properties. *J. Mater. Sci.*, 2006, **41**, 3845–3851.
7. Kirkpatrick, S., Percolation and conduction. *Rev. Mod. Phys.*, 1973, **45**, 574–588.
8. Jonscher, A. K., The universal dielectric response. *Nature*, 1977, **267**, 673–679.
9. Bergman, D. J. and Imry, Y., Critical behavior of the complex dielectric constant near the percolation threshold of a heterogeneous material. *Phys. Rev. Lett.*, 1977, **39**, 1222–1225.
10. Grannan, D. M., Garland, J. C. and Tanner, D. B., Critical behavior of the dielectric constant of a random composite near the percolation threshold. *Phys. Rev. Lett.*, 1981, **46**, 375–378.
11. Pecharromán, C., Esteban-Betegón, F., Bartolomé, J. F., López-Esteban, S. and Moya, J. S., New percolative $BaTiO_3$–Ni composites with a high and frequency-independent dielectric constant ($\varepsilon_r \approx 80\,000$). *Adv. Mater.*, 2001, **13**, 1541–1544.
12. Chen, Z., Huang, J., Chen, Q., Song, C., Han, G., Weng, W. and Du, P., A percolative ferroelectric–metal composite with hybrid dielectric dependence. *Scripta Mater.*, 2007, **57**, 921–924.
13. Huang, J., Cao, Y. and Hong, M., Ag–$Ba_{0.75}Sr_{0.25}TiO_3$ composites with excellent dielectric properties. *Appl. Phys. Lett.*, 2008, **92**, 022911.
14. Lin, Y., Nan, C.-W., Wang, J., Liu, G., Wu, J. and Cai, N., Dielectric behavior of $Na_{0.5}Bi_{0.5}TiO_3$-based composites incorporating silver particles. *J. Am. Ceram. Soc.*, 2004, **87**, 742–745.
15. López-Estebana, S., Bartoloméa, J. F., Pecharromána, C., Mello Castanhob, S. R. H. and Moya, J. S., Wet processing and characterization of ZrO_2/stainless steel composites: electrical and mechanical performance. *Mater. Res.*, 2001, **4**, 217–222.
16. Xiang, P.-H., Kinemuchi, Y. and Watari, K., Enhanced dielectric properties of bismuth titanate/silver composites. *J. Electroceram.*, 2006, **17**, 861–865.
17. Flaschen, S. S., An aqueous synthesis of barium titanate. *J. Am. Chem. Soc.*, 1955, **77**, 6194.
18. Kiss, K., Meander, J., Vukasovich, M. S. and Lockhart, R. J., Ferroelectric of ultrafine particle size. I. Synthesis of titanate powders of ultrafine particle size. *J. Am. Ceram. Soc.*, 1966, **49**, 291–294.
19. Chaput, F. and Boilot, J.-P., Alkoxide–hydroxide route to synthesize $BaTiO_3$-based powders. *J. Am. Ceram. Soc.*, 1990, **73**, 942–948.

20. Hayashi, T., Shinozaki, H. and Sasaki, K., Preparation and properties of $(Ba_{0.7}Sr_{0.3})TiO_3$ powders and thin films using precursor solutions formed from alkoxide–hydroxide. *J. Eur. Ceram. Soc.*, 1999, **19**, 1011–1016.
21. Pinceloup, P., Courtois, Ch., Vicens, J., Leriche, A. and Thierry, B., Evidence of a dissolution-precipitation mechanism in hydrothermal synthesis of barium titanate powders. *J. Eur. Ceram. Soc.*, 1999, **19**, 973–977.
22. Yoon, S., Baik, S., Kim, M. G. and Shin, N., Formation mechanisms of tetragonal barium titanate nanoparticles in alkoxide–hydroxide sol-precipitation synthesis. *J. Am. Ceram. Soc.*, 2006, **89**, 1816–1821.
23. Yoon, S., Baik, S., Kim, M. G., Shin, N. and Kim, I., Synthesis of tetragonal barium titanate nanoparticles via alkoxide–hydroxide sol-precipitation: effect of water addition. *J. Am. Ceram. Soc.*, 2007, **90**, 311–314.
24. Rodriguez-Carvajal, J., FULLPROF: a program for Rietveld refinement and pattern matching analysis. In *Abstracts of the Satellite Meeting on Powder Diffraction of the XV Congress of the IUCr*, 1990, p. 127.
25. Qi, J., Li, L., Wang, Y. and Gui, Z., Preparation of nanoscaled $BaTiO_3$ powders by DSS method near room temperature under normal pressure. *J. Cryst. Growth*, 2004, **260**, 551–556.
26. Kumar, V., Solution-precipitation of fine powders of barium titanate and strontium titanate. *J. Am. Ceram. Soc.*, 1999, **82**, 2580–2584.